GEOPHYSICAL RESEARCH LETTERS, VOL. 37, L05602, doi:10.1029/2009GL042359, 2010

Coincident reflection images of the Gulf Stream from seismic and hydrographic data

R. Mirshak,[1] M. R. Nedimović,[1,2] B. J. W. Greenan,[3] B. R. Ruddick,[4] and K. E. Louden[4]

Received 31 December 2009; revised 25 January 2010; accepted 1 February 2010; published 5 March 2010.

[1] The development of seismic oceanography requires direct comparison of seismic data to high-resolution oceanographic measurements over long horizontal scales. Here, we compare multichannel seismic (MCS) reflection images to 300 km of spatially-coincident, high-resolution (<1 km) expendable bathythermograph (XBT) surveys that were collected near a frontal region of the Gulf Stream. Fronts, eddies, tendrils, and interleaving were among the features identified in both data sets. In some cases, identification of features would be difficult if only hydrographic data were collected at conventional spatial scales. Comparing MCS reflection images with others derived purely from hydrographic data reveal many similarities and show that interleaving can be clearly identified with seismic methods. Varied time lags between MCS and hydrographic data collection identified the need for the separation between collecting both data sets to be short (i.e. hours to days), with advective processes and decorerlation time scales of desired features affecting acceptable sampling strategies. **Citation:** Mirshak, R., M. R. Nedimović, B. J. W. Greenan, B. R. Ruddick, and K. E. Louden (2010), Coincident reflection images of the Gulf Stream from seismic and hydrographic data, *Geophys. Res. Lett.*, *37*, L05602, doi:10.1029/2009GL042359.

1. Introduction

[2] Multichannel seismic (MCS) methods provide the potential of realizing long sections of near-synoptic 2D and swath 3D images of ocean fine structure [*Holbrook et al.*, 2003]. Although these methods are well established in relatively stationary solid earth settings, a number of fundamental questions concerning their application to oceanography remain unanswered, and many oceanographers remain undecided on the utility of MCS methods as an oceanographic tool. As a result, there continues to be a need to further document the capabilities and limitations of MCS methods in oceanographic analysis.

[3] It has been demonstrated that seismic reflections can correlate well with vertical temperature structure [*Nandi et al.*, 2004; *Nakamura et al.*, 2006], providing the possibility of capturing the temperature gradient [*Páramo and Holbrook*, 2005] and potentially the temperature profile itself [*Wood et al.*, 2008]. In addition, it has been suggested that horizontal wave number spectra of reflectors in seismic images may be capable of providing insights into the oceanic internal wave energies [*Holbrook and Fer*, 2005] and turbulent dissipation [*Klymak and Moum*, 2007]. However, it is not known how different oceanographic features manifest themselves in MCS data [*Ruddick et al.*, 2009] nor how a dynamic environment will affect MCS reflection imaging. For oceanographers to cast judgement on seismic oceanography (SO), detailed groundtruthing, particularly in areas of strong currents, is necessary.

[4] Here, we report results from a joint oceanographic and seismic survey, the Reflection Ocean Seismic Experiment (ROSE), which took place near a front between Gulf Stream waters and cold slope waters southeast of Nova Scotia, Canada (Figure 1). The study included what we believe is an unprecedented density of expendable bathythermograph (XBT) casts (average spacing between successive launches was <1 km along ~330 km of spatially coincident MCS transects). The XBT data were combined with CTD casts collected during the survey to produce hydrographically-derived reflection images that are compared to MCS reflection imagery.

2. Methods

[5] Data were collected from two sampling platforms, the *GSI Pacific* (MCS data) and the R/V *Endeavor* (hydrographic data), along two transects: Line 708 and Line 709 (Figure 1). Here we present a subsection of the data, selecting features that are particularly noteworthy of discussion.

[6] Leg A of Line 708 began with the oceanographic ship regularly deploying XBTs while trailing the seismic ship by ~10 km (~1 hour). This distance changed in time as the oceanographic vessel stopped to perform CTD casts then increased speed (while continuing XBT sampling) to catch up to the seismic vessel. Timing most CTD casts with interruptions in seismic data collection minimized the temporal separation between the spatially coincident seismic and XBT data collection. After ~150 km, the oceanographic vessel broke course and performed a reverse transect (Leg B) to examine how temporal effects might influence the seismic sampling in this active region (Figure 1). The oceanographic vessel then proceeded to perform a CTD/XBT survey along Line 709 (in a region with much weaker currents) about 1.5 days prior to the seismic survey along the same transect (Figure 1).

[7] During sampling, the *Endeavor* was deploying Sippican T-5 XBTs every six minutes, corresponding to a spatial separation of between 500 m and 1500 m, depending on the speed of the ship and the direction of travel relative

[1]Department of Earth Sciences, Dalhousie University, Halifax, Nova Scotia, Canada.
[2]Lamont-Doherty Earth Observatory of Columbia University, Palisades, New York, USA.
[3]Bedford Institute of Oceanography, Fisheries and Oceans Canada, Dartmouth, Nova Scotia, Canada.
[4]Department of Oceanography, Dalhousie University, Halifax, Nova Scotia, Canada.

0094-8276/10/2009GL042359$05.00

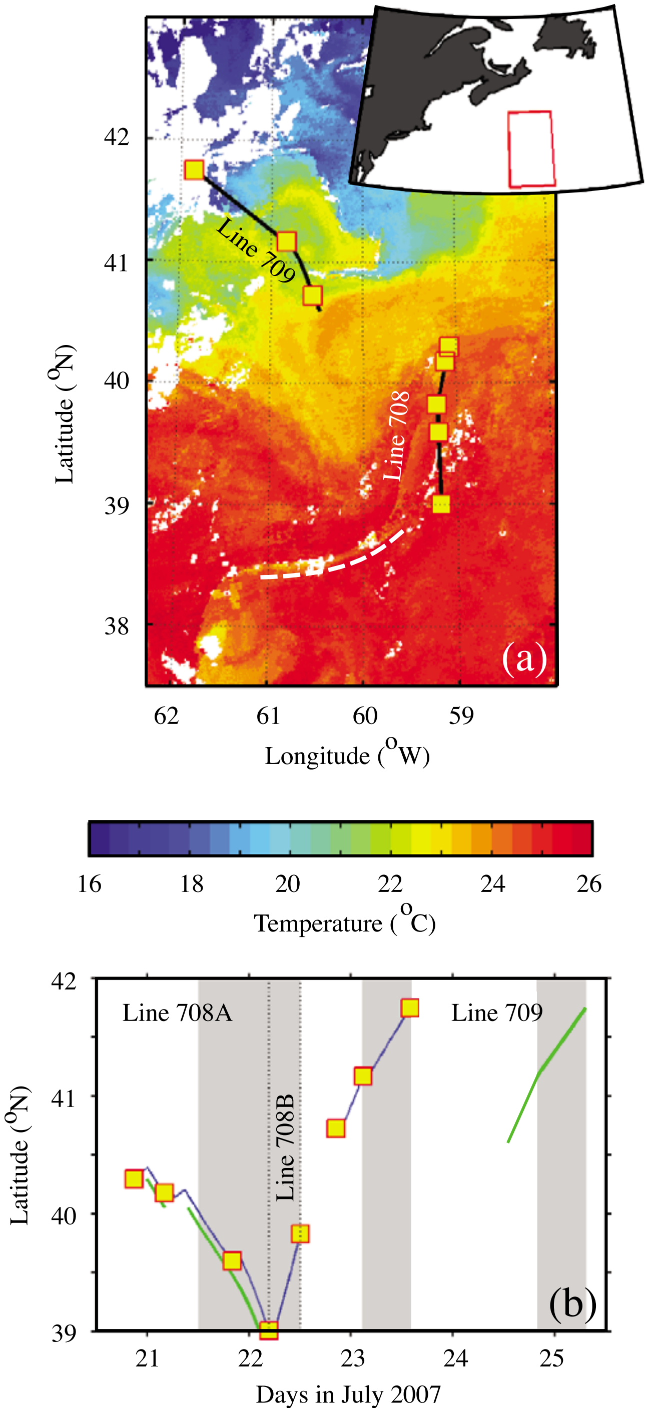

Figure 1. Coincident MCS and hydrographic surveys in space and time. (a) Location of Lines 708 (south) and 709 (north) displayed over a temporally coincident SST image. The white dashed line shows the feature thought to be related to the tendril seen on Line 708A. The inset shows the geographic setting of the study region. (b) Timing of sampling for the GSI Pacific (green) and R/V Endeavor (blue). The thin dashed lines separate Line 708A, Line 708B, and Line 709. Parts of transects shown in Figures 2 to 4 are marked with a gray background. Yellow squares represent CTD casts.

to ocean currents. Altogether, 490 XBTs were deployed along ~330 km of transect lines that were spatially coincident with the ongoing MCS survey. The *Endeavor* stopped eight times to perform CTD casts to a depth of 1500 m (Figure 1). The *Endeavor* also had a hull-mounted 75 kHz acoustic Doppler current profiler (ADCP) that recorded horizontal velocities to a depth of 700–800 m.

[8] Seismic energy was generated on the *GSI Pacific* by a 4410 cu. in. (70 l) tuned air gun array that was fired at 50 m intervals, with returns recorded digitally on a 4 km-long streamer with 320 hydrophone groups. The sample rate and listening time were 2 ms and 16 s, respectively. The seismic reflection images were produced using standard techniques that included geometry definition, common midpoint (CMP) sorting, and stacking. (For more information on seismic data analysis techniques, see *Yilmaz* [2001].) Data were bandpass filtered in frequency and wave number space to reduce noise and reverberations, and arrival times were adjusted to consider the sound speed variation and the varying ray path geometry.

[9] In essence, water column reflection images are derived from the convolution of the acoustic source wavelet W with the acoustic reflectivity of the water column R, i.e. $W * R$. Seismic reflection sections derived from oceanographic data were created by convolving R-values extracted from the hydrographic data with an estimate of W provided by Geophysical Services Incorporated (GSI). For each XBT profile (i) and depth horizon (j), $R_{i,j}$ was calculated as

$$R_{i,j} = \frac{Z_{i,j+1} - Z_{i,j-1}}{Z_{i,j+1} + Z_{i,j-1}} \qquad (1)$$

where $Z_{i,j} = c_{i,j}\rho_{i,j}$ is acoustic impedance, $c_{i,j}$ is the propagation speed of sound, and $\rho_{i,j}$ is density [*Yilmaz*, 2001]. Note that in the ocean, changes in Z are small, so in this environment R is essentially a scaled gradient of Z.

[10] The values of c and ρ were estimated as follows. Smoothed (4th-order Butterworth filter with a cut-off wavelength of 5 m) density profiles were extracted from CTD casts bracketing each set of XBT transects. Each bracketing pair of density profiles were averaged, thereby providing a "representative" density-profile across the section. Assuming no horizontal density gradient, estimates of salinity were derived from the XBT temperature field by inverting the equation of state. This approach permitted approximation of $\rho = \rho(S, T, p)$ and $c = c(S, T, p)$ for each XBT cast. While this method does not provide the precise values of ρ and c, approximately 90% of the variance in R is derived from gradients in temperature [*Sallarés et al.*, 2009]. Based on the above factors, the error in R due to salinity estimation (δR) is expected to be at second-order, i.e. $\delta R/R \ll 0.1$.

3. Observations

3.1. Line 708

[11] Figure 2 shows oceanographic and seismic data collected on the southern half of Line 708A (Figure 1). The thermocline, situated near the 18°C isotherm, is marked by a strong reflector, which deepens by about 200 m across the part of Line 708A shown in Figure 2. The red and blue in the reflection images represent negative and positive reflection amplitudes respectively that are the result of

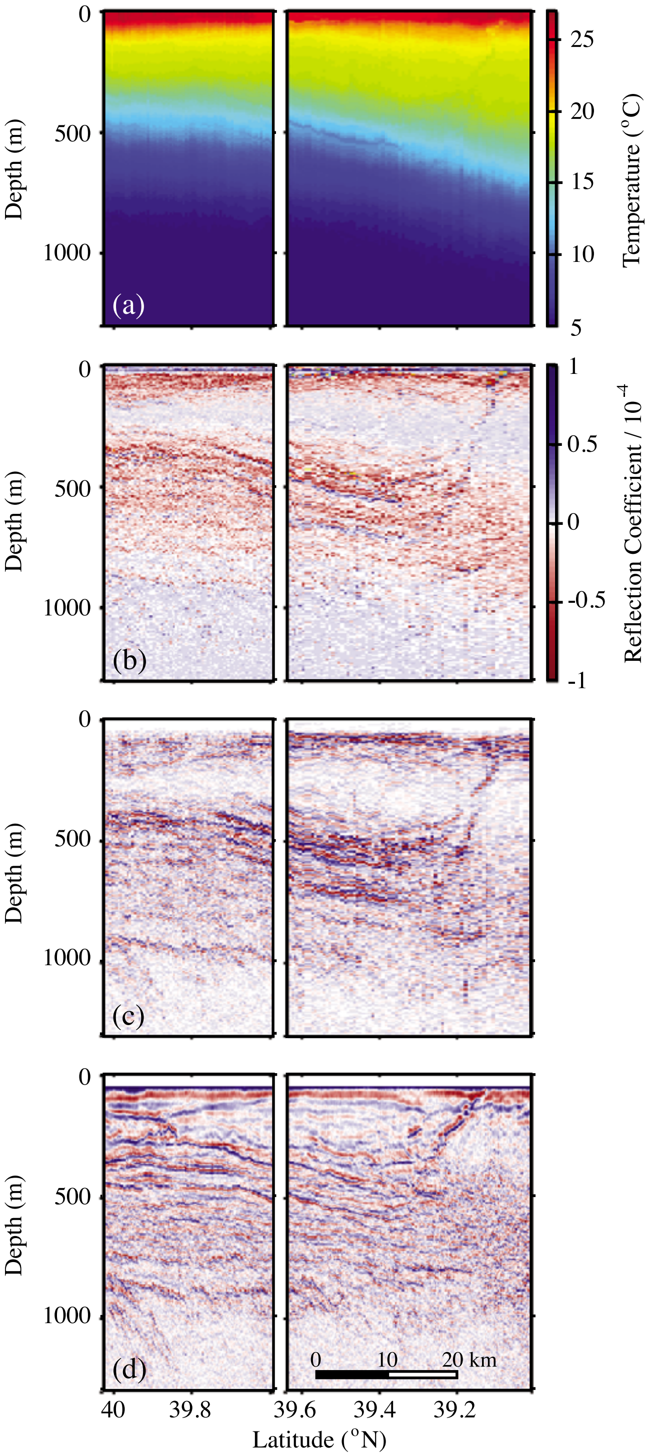

Figure 2. Oceanographic and seismic data along Line 708A. (a) Temperature from XBT casts. (b) Reflection coefficient inferred from hydrographic data. (c) Inferred reflection image generated by convolving inferred reflection coefficient with estimate of source wavelet. (d) MCS reflection image. Vertical gap between panels indicates timing of a CTD cast, which disturbed the continuity of the oceanographic transects.

convolving the source wavelet (which has a peak and trough) with the reflectivity profile [e.g., *Yilmaz*, 2001]). Qualitative differences between Panels c and d, such as the sharpness of the thermocline, are likely due to a number of factors including the inaccuracy of the estimated source wavelet and the relative simplicity of the convolution model used to produce the hydrographically-derived image compared to the involved processing stream required for the MCS image.

[12] The water above the thermocline is comparatively homogeneous in temperature, resulting in weak reflection coefficients within the layer. Although not shown in Figure 2, XBT data collected further North on Line 708 show a frontal feature as the thermocline depth reduces to about 200 m by 40.35°N. (The advected front is present on Line 708B, discussed below.)

[13] Towards the southern end of the transect (39.2°N at about 200 m depth) the reflection coefficient and reflection images show a coherent dipping structure, possibly a tendril of cooler water related to the cold feature near 61.5°W, 37.75°N (Figure 1). The signal is captured by the dense XBT survey, but it could not be identified in the ADCP data, likely because density compensation reduced any change in currents to an undetectable level. It is thus unlikely that this feature would have been identified without the high-resolution data collected here.

[14] The hydrographic data collected on Line 708A are compared to those from Line 708B in Figure 3. The differences between the two lines are due to the temporal shift between them, which varied from 2 h at the south end to 12 h at the north end. The change is consistent with a lateral shift of a Gulf Stream meander within this time period, a phenomenon frequently observed in the area during the summer months [*Watts and Johns*, 1982]. The temporal variation in temperature along the transect is displayed in Figures 3d and 3e, with the movement of the front shown by the depth of the 16°C isotherm on the two lines. After stopping to make the CTD cast (105 min) at the end/beginning of Line 708A/B, there is little change within the top 500 m of the water column. As the lag between the two lines increased, the change remained small until 4.5 hours, after which the front (not shown for Line 708A) began to cross Line 708B.

3.2. Line 709

[15] Figure 4 compares the oceanographic and seismic data from Line 709. Despite the seismic survey lagging the hydrographic survey by over 30 h (Figure 1), a number of correlatable features from the near-surface down to 1200 m depth are visible in both surveys. Unlike the data collected on Line 708, where a shorter time-lag in the energetic Gulf Stream led to decorrelation between Legs A and B, features on Line 709 remained present over a longer period of time, consistent with the expected displacement timescales of such features [*Watts and Johns*, 1982].

[16] Near the surface, a warm water lens is visible in the temperature cross-section. The temperature data indicate that a tongue of cold water is wrapping around the southern edge of the eddy, consistent with the cold slope water seen just east of the transect in Figure 1.

[17] Below the eddy (near 41.5°N), a set of reflectors is coherent from a depth of 500 m down to 1200 m. These reflectors are similar to an unexplained feature seen in

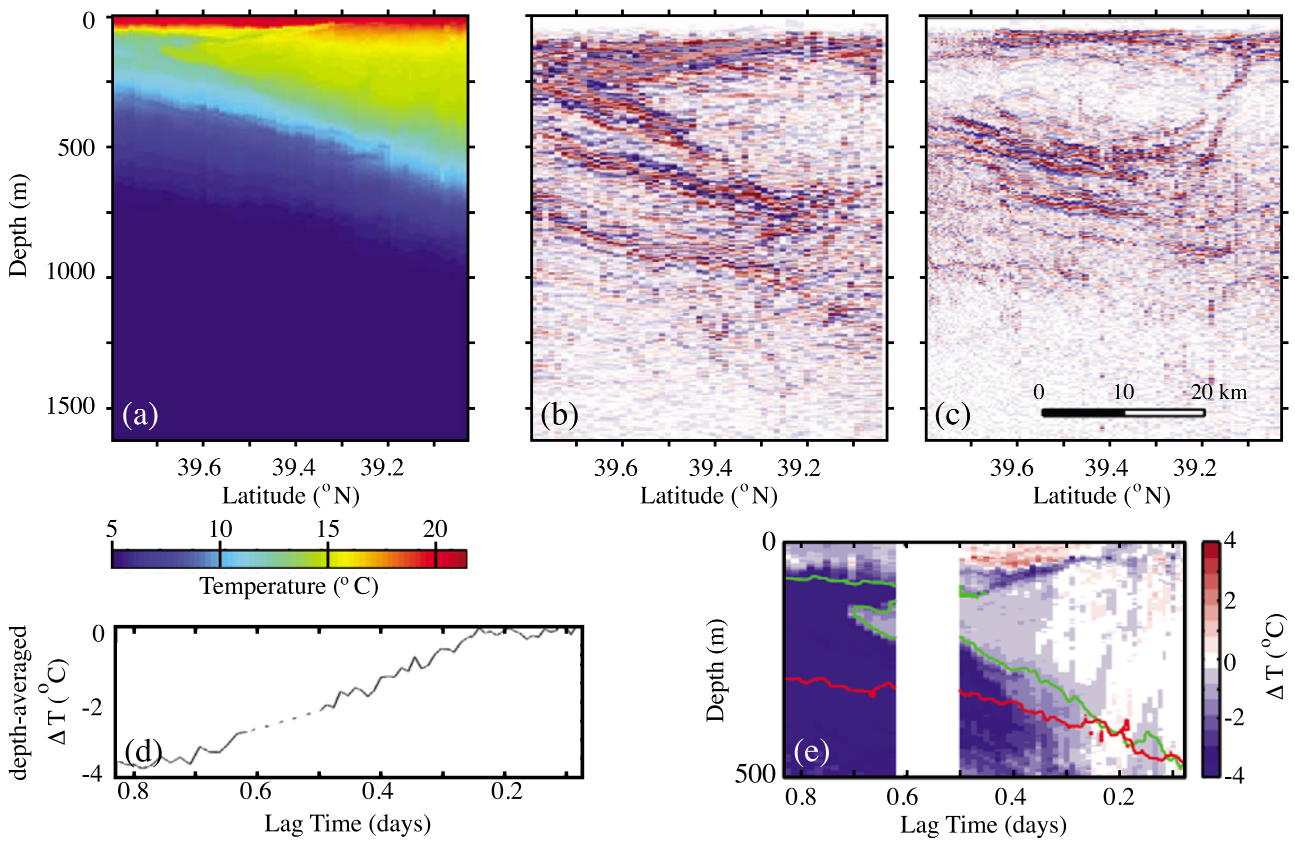

Figure 3. Oceanographic data along Line 708. (a and b) XBT data and hydrographically-derived reflection image for Line 708B. (c) The hydrographically-derived reflection image on Line 708A. Temperature difference between Lines 708B and 708A as a function of time lag between XBT casts is shown for (d) depth-averaged to 500 m and (e) vertical section. (e) The contours show the depth of the 16°C isotherm for Lines 708A (red) and 708B (green).

Figure 3 of *Holbrook et al.* [2003]. While the source of such features was speculated [*Holbrook et al.*, 2003], the direct comparison with ocean temperature data here provides strong evidence that they are the signature of interleaving (see the inset in Figure 4a). This interpretation is consistent with the seismic image, which suggests a ~10 km-wide band of near-horizontal, layered reflectors. While the eddy maintains its location over the 30 h lag between the two transects, the interleaving feature appears to shift north. Further south, at 41.2°N, another feature is visible in the MCS imagery between about 600 m and 1000 m depth. A similar feature could not be identified in the hydrographic data, suggesting that it was advected onto the transect line between the XBT and MCS surveys.

4. Discussion and Conclusions

[18] The reflection images calculated from seismic and oceanographic data share a number of common features, ranging from the mesoscale (e.g. fronts and eddies) to scales of a few km (e.g. tendrils and interleaving features). The similarity between the seismic and hydrographically-derived reflection images provide strong supporting evidence that the MCS techniques can be used to image oceanic features, allowing inference of processes at horizontal resolution far beyond what is available with more conventional oceanographic sampling methods.

[19] On Line 708A, at 39.3°N, a strong and coherent reflector, presumed to be a tendril from a parcel of cold water to the south, is present in both reflection images. This feature would most likely be missed in conventional oceanographic sampling due to its short length scales, both horizontally and vertically. Similarly, in the absence of the hydrographic data, the seismic image alone might suggest an eddy-like feature extending from 39.2°N to 39.9°N. By examining the seismic and hydrographic data sets together, we are able to propose that this feature is a tendril of cooler water being stirred by horizontal mixing processes of the Gulf Stream.

[20] Combining both data sets proved exceptionally useful in the identification of interleaving (Figure 4). The zig-zag nature characteristic of the temperature (and salinity) profiles displaying this phenomenon can be expected to produce a series of horizontal reflectors like those seen in the seismic images on Line 709. Positively identifying such features in hydrographic data is relatively straightforward, but determining their presence and identifying their slopes and length scales depends on the location and density of sampling relative to the features. The identification of interleaving at depth using 2D, or preferably 3D, MCS surveys could be used to advance our understanding of the frequency, patchiness, scales, and dynamics of this deep ocean mixing process.

[21] Temporal effects varied considerably between the two lines examined in this study. On Line 708, a change of

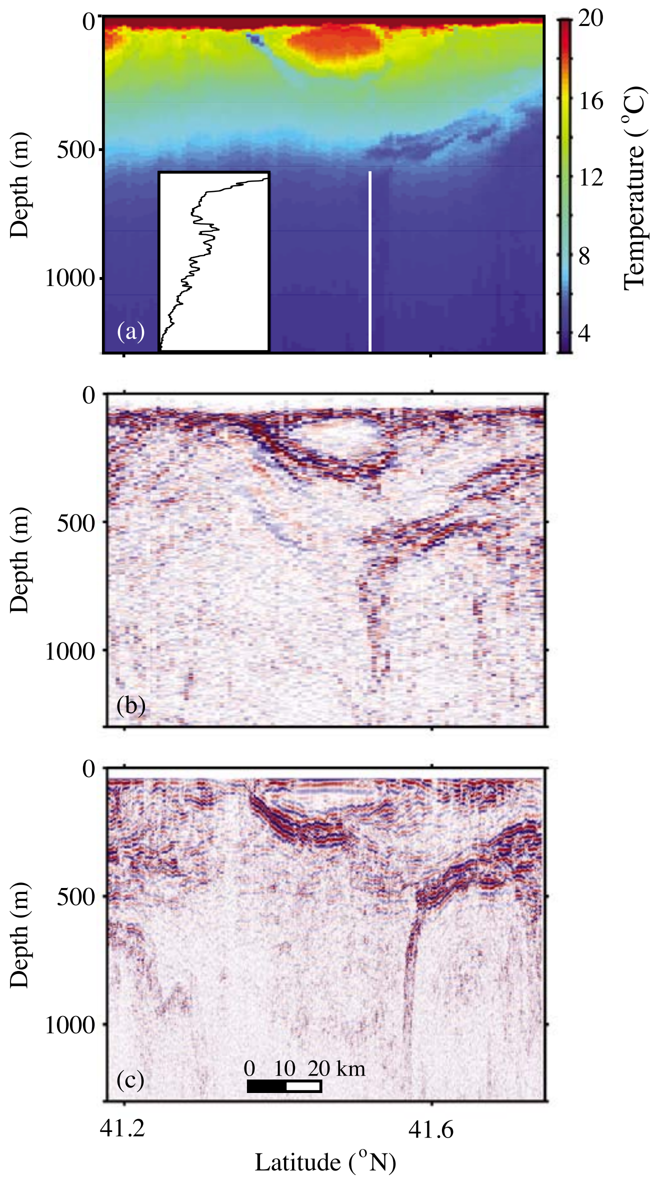

Figure 4. Oceanographic and seismic data along Line 709. (a) Temperature from XBT casts. (b) Reflection image based on XBT data. (c) MCS reflection image. In Figure 4a the inset shows the temperature profile at the location of the vertical white line, with the temperature range of the inset being from 4°C to 5°C.

O(10 h) showed a remarkable difference in the imaged structures (Figure 3), presumably due to advective processes in the region. In contrast to the variability on Line 708, the seismic and hydrographic sections on Line 709 were collected more than 24 h apart but the reflection images share a strong resemblance. The colder surface waters (Figure 1) and the ADCP data suggest that this section was further from the core of the Gulf Stream, and that currents were calmer. Thus, the time lag separating seismic and hydrographic sampling should not exceed the decorrelation time scales of the targeted features. This result underlines the importance of understanding the physical oceanographic setting when planning seismic surveys and interpreting the resulting seismic sections.

[22] In this work, we have used a combination of hydrographic and MCS data to identify some capabilities and limitations of SO. Differences between MCS and hydrographically derived refection images show how the timing of data collection and the data processing algorithms can impact the imaging results. While simultaneous collection of hydrographic data is ideal, introducing a lag between hydrographic and seismic data collection is acceptable for qualitative comparisons and feature identification, provided that the lag does not exceed the decorrelation scales of the structures of interest. In cases where this requirement was met, a number of features including eddies, tendrils, and interleaving were identified in both data sets. An interleaving structure, observed in both the seismic and hydrographic data sets, highlights how SO can be used to positively identify hard-to-capture oceanographic features.

[23] **Acknowledgments.** The Editor and anonymous reviewers provided valuable comments during the review process. Seismic data were kindly provided by the Natural Resources Canada Earth Sciences Sector. The SST data in Figure 1 were processed by Cathy Porter. This work was funded by an NSERC Special Research Opportunities grant.

References

Holbrook, W. S., and I. Fer (2005), Ocean internal wave spectra inferred from seismic reflection transects, *Geophys. Res. Lett.*, *32*, L15604, doi:10.1029/2005GL023733.

Holbrook, W. S., P. Páramo, S. Pearse, and R. W. Schmitt (2003), Thermohaline fine structure in an oceanographic front from seismic reflection profiling, *Science*, *301*, 821–824, doi:10.1126/science.1085116.

Klymak, J. M., and J. N. Moum (2007), Interpreting spectra of horizontal temperature gradients in the ocean: Part II - Turbulence, *J. Phys. Oceanogr.*, *37*, 1232–1245, doi:10.1175/JPO3074.1.

Nandi, P., W. S. Holbrook, S. Pearse, and R. W. Schmitt (2004), Seismic reflection imaging of water mass boundaries in the Norwegian Sea, *Geophys. Res. Lett.*, *31*, L23311, doi:10.1029/2004GL021325.

Nakamura, Y., T. Noguchi, T. Tsuji, S. Itoh, H. Niino, and T. Matsuoka (2006), Simultaneous seismic reflection and physical oceanographic observations of oceanic fine structure in the Kuroshio extension front, *Geophys. Res. Lett.*, *33*, L23605, doi:10.1029/2006GL027437.

Páramo, P., and W. S. Holbrook (2005), Temperature contrasts in the water column inferred from amplitude-versus-offset analysis of acoustic reflections, *Geophys. Res. Lett.*, *32*, L24611, doi:10.1029/2005GL024533.

Ruddick, B. R., H. B. Song, C. Z. Dong, and L. Pinheiro (2009), Water column seismic images as maps of temperature gradient, *Oceanography*, *22*, 192–205.

Sallarés, V., B. Biescas, G. Buffett, R. Carbonell, J. J. Daobeitia, and J. L. Pelegr (2009), Relative contribution of temperature and salinity to ocean acoustic reflectivity, *Geophys. Res. Lett.*, *36*, L00D06, doi:10.1029/2009GL040187.

Watts, D. R., and W. E. Johns (1982), Gulf Stream Meanders: Observations on Propagation and Growth, *J. Geophys. Res.*, *87*, 9467–9476, doi:10.1029/JC087iC12p09467.

Wood, W. T., W. S. Holbrook, M. K. Sen, and P. L. Stoffa (2008), Full waveform inversion of reflection seismic data for ocean temperature profiles, *Geophys. Res. Lett.*, *35*, L04608, doi:10.1029/2007GL032359.

Yilmaz, O. (2001), *Seismic Data Analysis: Processing, Inversion, and Interpretation of Seismic Data*, *Invest. Geophys. Ser.*, vol. 10, 2nd ed., edited by S. M. Doherty, Soc. of Explor. Geophys., Tulsa, Okla.

R. Mirshak and M. R. Nedimović, Department of Earth Sciences, Dalhousie University, 1355 Oxford St., Halifax, NS B3H 4J1, Canada. (ramzi@dal.ca)

B. J. W. Greenan, Bedford Institute of Oceanography, Fisheries and Oceans Canada, PO Box 1006, Dartmouth, NS B2Y 4A2, Canada.

K. E. Louden and B. R. Ruddick, Department of Oceanography, Dalhousie University, 1355 Oxford, Halifax, NS B3H 4J1, Canada.